基于法布里-珀罗腔产生飞秒激光脉冲串在硅表面诱导高质量亚波长周期条纹(特邀)

许宇锋,张羽婵,蒋其麟,沈辉辉,贾天卿
(华东师范大学 精密光谱科学与技术国家重点实验室,上海 200241)

摘　要:为了制备高质量表面周期结构,利用法布里-珀罗腔对飞秒激光进行时域整形,输出子脉冲间隔在 1~300 ps 内灵活可调的飞秒激光脉冲串,在硅表面诱导亚波长周期条纹。实验结果显示,利用飞秒激光脉冲串诱导得到的亚波长周期条纹明显优于原始高斯光诱导的亚波长周期条纹。利用子脉冲间隔为 100 ps 的脉冲串诱导的亚波长条纹最佳,条纹周期为 1 008 nm,结构取向角为 2.8°,边缘粗糙度为 3.9 nm,可达到光刻工艺的标准。

关键词:激光加工;激光诱导表面周期结构;亚波长周期条纹;法布里-珀罗腔;飞秒激光脉冲串;硅

中图分类号:TN244　　　　**文献标识码**:A　　　　**doi**:10.3788/gzxb20235207.0752301

0 引言

飞秒激光诱导表面周期结构(Laser-induced Periodic Surface Structures, LIPSS)能够广泛应用于不同加工领域[1],涉及半导体[2-4]、电介质[5-7]、金属[8-10]、聚合物[11, 12]等各种材料。LIPSS现主要分为两类:周期 Λ 大于 $\lambda/2$ 的亚波长条纹(Near-Subwavelength Ripples, NSRs)和周期 Λ 小于 $\lambda/2$ 的深亚波长条纹(Deep-Subwavelength Ripples, DSRs),其中 λ 为入射激光波长。过去几十年里,随着理论以及实验工作的深入,研究人员观察到这种周期性微纳结构可以改善材料表面性能,可用于材料表面浸润性调控[13-15]、增强表面拉曼散射[16, 17]、表面结构色[2, 18]、双折射[19, 20]和光存储[21]等,在数据存储、工业制造、生物医学等领域都有广泛应用。

通常认为,NSRs是由入射光激发材料表面等离激元(Surface Plasmon Polaritons, SPP),使得激光能量在材料表面周期性分布的结果[22-24]。诱导高质量NSRs目前还存在诸多问题,例如SPP激发弱导致周期性能量沉积不足,条纹浅;剩余热效应较大,条纹易出现分叉,扭曲,甚至被淹没;加工过程中碎屑沉积,条纹粗糙,颗粒感重。为了得到均匀性好、规则性高的高质量NSRs,首要任务是控制和增强SPP。CAO Kaiqiang等[25]利用双光束干涉共振增强SPP激发,在硅上加工出了大面积均匀光栅。JALIL S A等[26]利用两路不同延迟时间的共线飞秒激光脉冲在镍表面制备出了高度均匀的大面积NSRs,认为这种高度均匀性来源于SPP传播长度的减小。

飞秒激光诱导周期性纳米结构的形成是一个复杂的过程。在飞秒激光照射到材料后的几纳秒内,会发生载流子激发、载流子升温、晶格升温、等离子体喷出、纳米颗粒喷出等一系列超快过程。通过脉冲整形能够调控激光能量在时域上的分布,进而调控激光与物质相互作用的超快过程,有效控制激光能量在材料表面的周期性沉积、剩余热效应以及诱导过程中沉积的碎屑,从而获得深度大、均匀性好的LIPSS。随着脉冲整形技术的发展,研究人员已经能够实现对飞秒激光时域上的任意调控,现有脉冲整形方法包括4f结构零

色散脉冲整形[2, 27, 28]、双折射晶体阵列产生脉冲串[29, 30]、类迈克尔逊干涉仪方法[31, 32]等。ZHANG Yuchan等[2]利用4f脉冲整形系统得到子脉冲间隔为16.2 ps的时域整形脉冲串,在硅表面制备了非常规则、深度大、面积大的NSRs。ZHANG Jin等[31]利用迈克尔逊干涉装置输出两列飞秒激光脉冲,通过改变脉冲延迟时间来控制聚丙乙烯微球内部的电离过程以改进激光加工。但这些时域整形方法都较为繁琐,且稳定性差,有待进一步发展。

基于法布里-珀罗(Fabry-Perot, F-P)腔的脉冲串产生装置光路易于调节、成本低并且较为稳定可靠。本文利用法布里-珀罗腔对飞秒激光进行时域整形,输出子脉冲间隔在1～300 ps内灵活可调的飞秒激光脉冲串。通过调控脉冲串的子脉冲间隔、加工扫描速度、激光能流密度等诱导NSRs,达到光刻工艺的标准[33]。

1 实验装置

图1为基于F-P腔飞秒激光脉冲串加工系统[34],利用激光器(Light Conversion, PHAROS)输出中心波长为1 030 nm,脉宽为250 fs,单脉冲能量为1 mJ,重复频率为5 kHz的飞秒激光脉冲。水平偏振的出射激光经格兰棱镜(Glan Polarizer, GP)后射入四分之一波片(Quarter Wave Plate, QWP)。四分之一波片的快轴与水平方向呈45°夹角,将水平偏振光调整为左旋偏振光(或者右旋偏振光),垂直射入F-P腔。入射激光经由F-P腔反射回四分之一波片,变为垂直偏振光,在格兰棱镜处发生反射,又经反射镜M1进入半波片(Half Wave Plate, HWP)。半波片用于调节激光偏振,使得激光偏振方向和样品移动方向平行。最后激光通过$f=50$ mm的柱面透镜(Cylindrical Lens, CL)汇聚到样品表面,焦斑尺寸为10 mm×50 μm,焦斑的长轴方向和样品移动方向垂直。实验中利用衰减片调节激光脉冲能量。利用三维电控平移台(XYZM148H-150D,上海联谊)移动样品,实现激光加工。用白光光源照明样品表面,对激光加工过程进行实时监控。
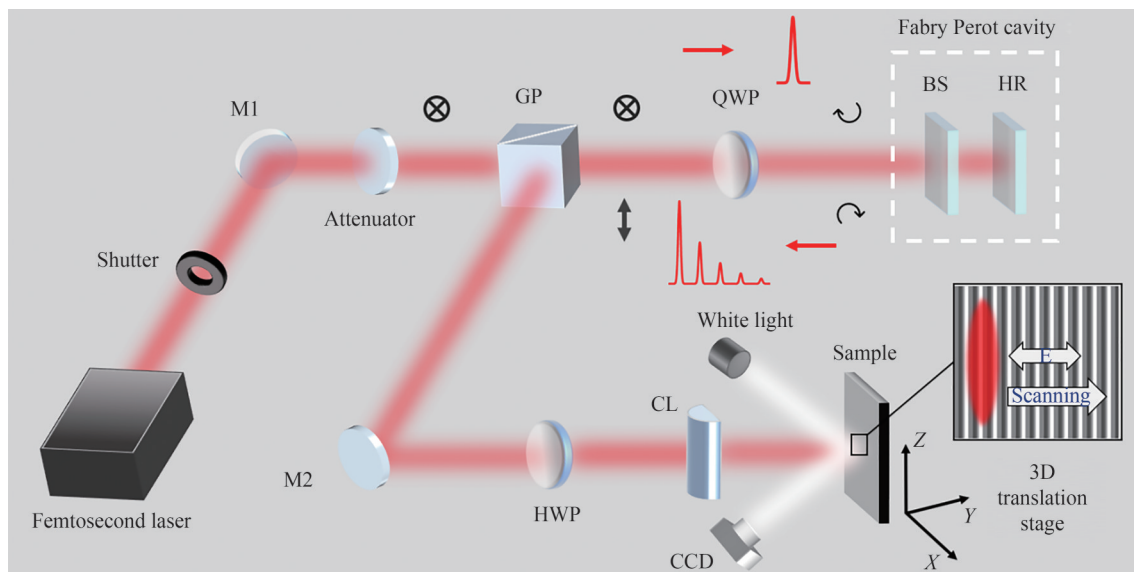

图1 F-P腔脉冲整形实验装置示意图
Fig.1 Schematic diagram of experimental device for pulse shaping of F-P cavity

实验样品为商用无掺杂硅晶片(MTI,中国),厚度为0.5 mm,粗糙度小于1 nm,单面抛光。样品加工结束后先使用10%浓度氢氟酸(HF)溶液浸泡90 min以去除表面氧化物和烧蚀碎屑,再经丙酮超声清洗30 min,最后用去离子水超声清洗30 min。样品处理完毕后利用扫描电子显微镜(Scanning Electron Microscope, SEM)(S-4800,日立)对样品表面形貌进行拍摄,利用白光干涉共聚焦显微镜(Smartproof 5 Widefield Confocal Microscope,蔡司)测量样品深度。

图2(a)所示为F-P腔产生脉冲串的原理示意图。F-P腔由一个反射透射比为5:5的平板分束片(Beam Spliter, BS)和一个零度高反镜组成。飞秒激光脉冲垂直入射到平板分束片上,反射光作为脉冲串的第一个子脉冲。透射光垂直入射到零度高反镜后又反射回平板分束片,再次发生反射、透射。此时透射光作为脉冲串的第二个子脉冲,反射光垂直射入零度高反镜,如此往复,输出子脉冲强度递减的飞秒激光脉冲串。脉

冲串中子脉冲间隔由平板分束片和零度高反镜之间的距离 d 决定,时间间隔 $\triangle t = 2d/c$,c 为光速。子脉冲的能量比与分束片的分束比有关。本文中利用的飞秒激光脉冲串的子脉冲的强度依次为 0.5、0.25、0.125、0.062 5……,通过改变平板分束片和零度高反镜之间的距离得到不同子脉冲间隔的飞秒激光脉冲串。图 2(b) 为 F-P 腔腔长为 7.5 mm 时得到子脉冲间隔 50 ps 脉冲串的光强时域分布。

(a) Schematic diagram of F-P cavity generating pulse train

(b) Temporal intensity profile of the shaped pulse of 50 ps
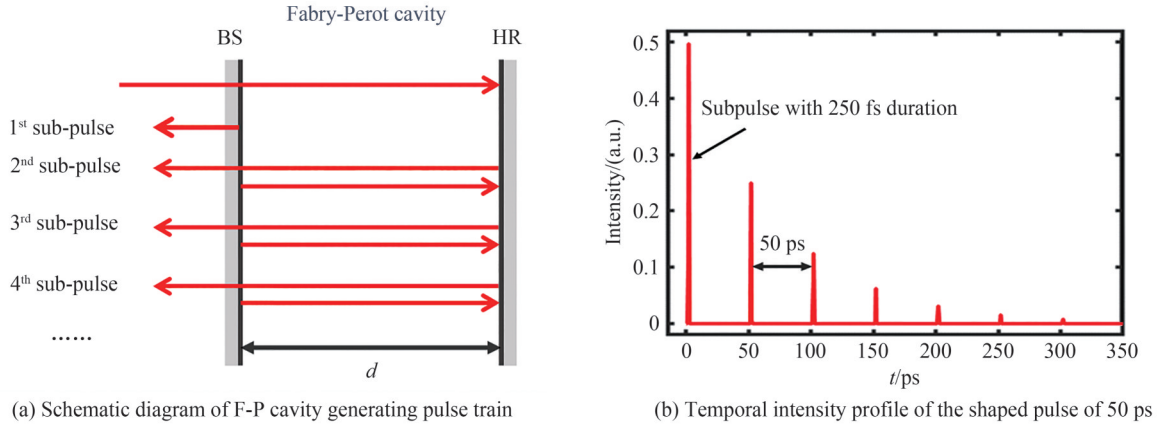
图 2　F-P 腔对飞秒激光时域整形

Fig.2　Femtosecond laser pulse train shaped by F-P cavity

2　实验结果

2.1　高斯激光脉冲诱导 NSRs

利用中心波长为 1 030 nm,重复频率为 5 kHz 的高斯飞秒激光脉冲,经柱透镜汇聚到硅片表面,诱导出大面积 LIPSS。激光偏振方向与扫描方向和柱透镜汇聚的焦斑短轴方向平行。当高斯激光脉冲作用在硅表面时,载流子瞬时吸收光子能量达到激发态,在表面形成 SPP 层;而后,电子通过电声耦合作用将能量传递给晶格,该过程约数十皮秒;最后,当晶格温度超过材料的烧蚀阈值,硅表层开始发生熔化、汽化等烧蚀过程。图 3 为不同扫描速度下,高斯激光脉冲诱导的最均匀的亚波长条纹。如图 3(a)所示,扫描速度较低为 0.1 mm/s 时,能流密度为 0.20 J/cm² 时,由于累积脉冲数过多,条纹交叉严重,边界不清晰,同时在部分亚波长条纹的脊上,由于能量局域增强,条纹产生分裂。图 3(b)所示,当扫描速度为 0.5 mm/s 时,材料表面可以

(a) v=0.1 mm/s, F=0.20 J/cm²

(b) v=0.5 mm/s, F=0.21 J/cm²

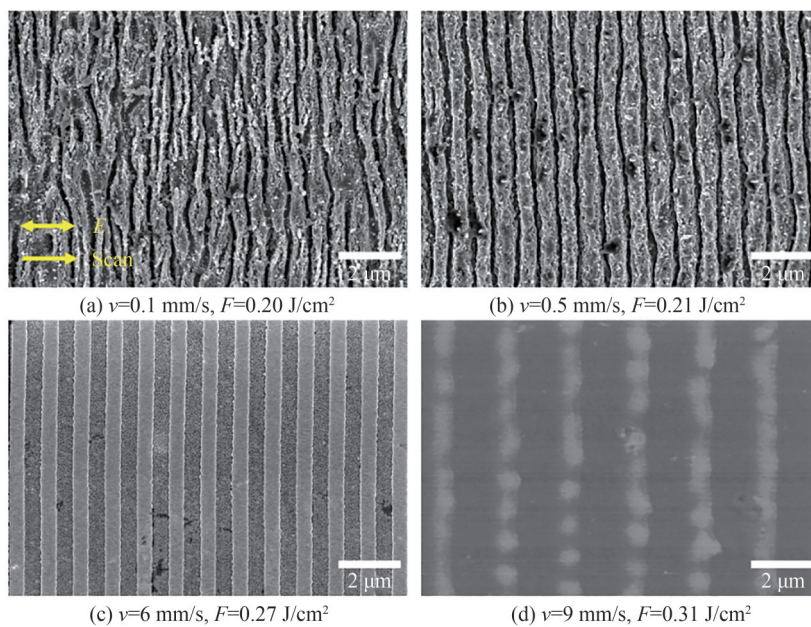(c) v=6 mm/s, F=0.27 J/cm²

(d) v=9 mm/s, F=0.31 J/cm²

图 3　不同扫描速度下高斯激光脉冲诱导均匀 NSRs 的扫描电镜照片

Fig.3　SEM images of regular NSRs induced by Gaussian laser pulse at different scanning velocity

形成较为均匀的亚波长周期条纹,周期$\varLambda=(731\pm36)$ nm。但由于脉冲累积数仍然较多,条纹烧蚀较重,发生一定程度弯曲,材料表面喷出物多,条纹边沿粗糙度高。如图3(c)所示,当扫描速度为6 mm/s时,能流密度为0.27 J/cm²时,高斯激光脉冲诱导出了均匀的亚波长条纹,周期$\varLambda=(1\,027\pm21)$ nm,条纹略微弯曲,整体取向较为一致。这是高斯激光脉冲在所有条件下诱导出的最规则条纹。如图3(d)所示,当扫描速度为9 mm/s时,由于扫描速度较大,脉冲累积数少,单位面积上沉积的激光能量较少,不足以诱导出连续的亚波长条纹,单根条纹上发生断裂,条纹之间凹槽深度变浅。

图4显示了高斯激光脉冲在硅上诱导不同形貌的NSRs的能流密度窗口。在0.1～4 mm/s扫描速度下,仅出现不连续或者部分烧坏的NSRs。随着扫描速度增大到5 mm/s时,规则NSRs开始出现。当扫描速度为6 mm/s时,诱导规则NSRs的能流密度窗口最大,为0.02 J/cm²(0.25～0.27 J/cm²)。当扫描速度达到9 mm/s时,样品表面仅能出现弯曲、断裂的条纹。总之,高斯激光脉冲诱导规则NSRs的能流密度窗口小,对激光脉冲能量的调控要求高,不易加工出大面积规则NSRs。
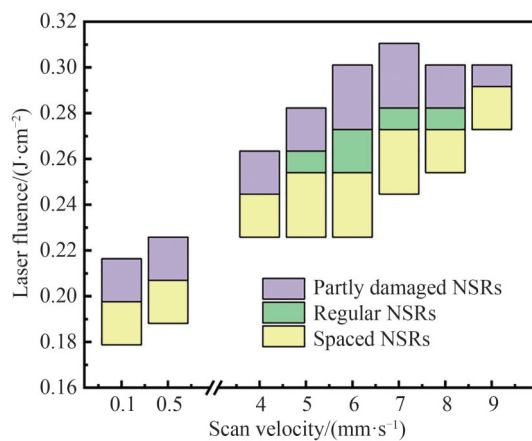

图4　高斯激光脉冲在硅上诱导不同形貌的NSRs的能流密度窗口

Fig.4　The laser fluence window of spaced, regular and partly damaged NSRs induced by Gaussian laser pulse on silicon

2.2　飞秒激光脉冲串诱导NSRs

图5所示为高斯飞秒激光脉冲和飞秒激光脉冲串能够诱导出的最规则NSRs的扫描电镜照片,扫描速度$v=6$ mm/s。激光偏振方向与扫描方向和柱透镜汇聚的焦斑短轴方向平行。如图5(a)所示,高斯激光脉冲条件下,条纹略微弯曲,边缘粗糙。当子脉冲间隔为50 ps时,如图5(b)所示,诱导的NSRs表面粗糙,条纹边沿呈锯齿状。当子脉冲间隔为100 ps时,条纹整体取向一致,边缘光滑、平直。对图5(c)进行傅里叶变化得到的空间频谱成分分布如图5(g)所示。水平方向频率分布如图5(h)所示,频谱峰值为(0.992 ± 0.008) μm⁻¹,对应周期$\varLambda=(1\,008\pm8)$ nm。随着子脉冲间隔增大,也可诱导出均匀条纹,如图5(d)所示。当子脉冲间隔增大到200 ps时,如图5(e)所示,单根条纹的粗细不均匀,整体开始变得弯曲,取向不一致。当子脉冲间隔为300 ps时,如图5(f)所示,单根条纹两侧呈锯齿状边缘,边缘粗糙度极大。

激光诱导表面周期结构是入射光激发SPP使得激光能量周期性沉积的结果[22-24]。SPP的波矢与入射光波矢不匹配[22],需要材料表面有部分介电常数突变区使得SPP和入射光矢量匹配,增强激光周期性沉积[10, 25]。对于高斯飞秒激光来说,通常需要前面多个脉冲烧蚀材料,使得材料表面出现烧蚀喷出物,满足诱导周期条纹的条件。而烧蚀喷出物严重影响了周期条纹的取向,使得条纹弯曲、分叉等。同时,飞秒激光烧蚀材料时发生的库伦爆炸[35]和热流体力学[36]等使得条纹边沿呈锯齿状,粗糙度高。

图6显示了飞秒激光脉冲串诱导规则NSRs形成过程的原理。当飞秒激光脉冲串照射材料后,第一个子脉冲作用在硅表面后,载流子浓度发生剧烈变化,迅速形成高密度自由电子层,光学性质由半导体变为类金属态,在表面形成瞬态条纹[37]。后续子脉冲持续作用时,由于光栅耦合效应[22],增强SPP的激发和激光能量沉积。此外,后续子脉冲进一步激发高热表面,使得高热材料喷发带走沉积热量,减小剩余热效应[38]。其次,后续子脉冲可以多次激发前序子脉冲烧蚀产生的喷出物,使其碎裂成更小尺寸的颗粒甚至是直接汽化。更多的激光能量周期性沉积和更小的热效应,以及更少的表面沉积颗粒,使得子脉冲间隔为100 ps的飞秒
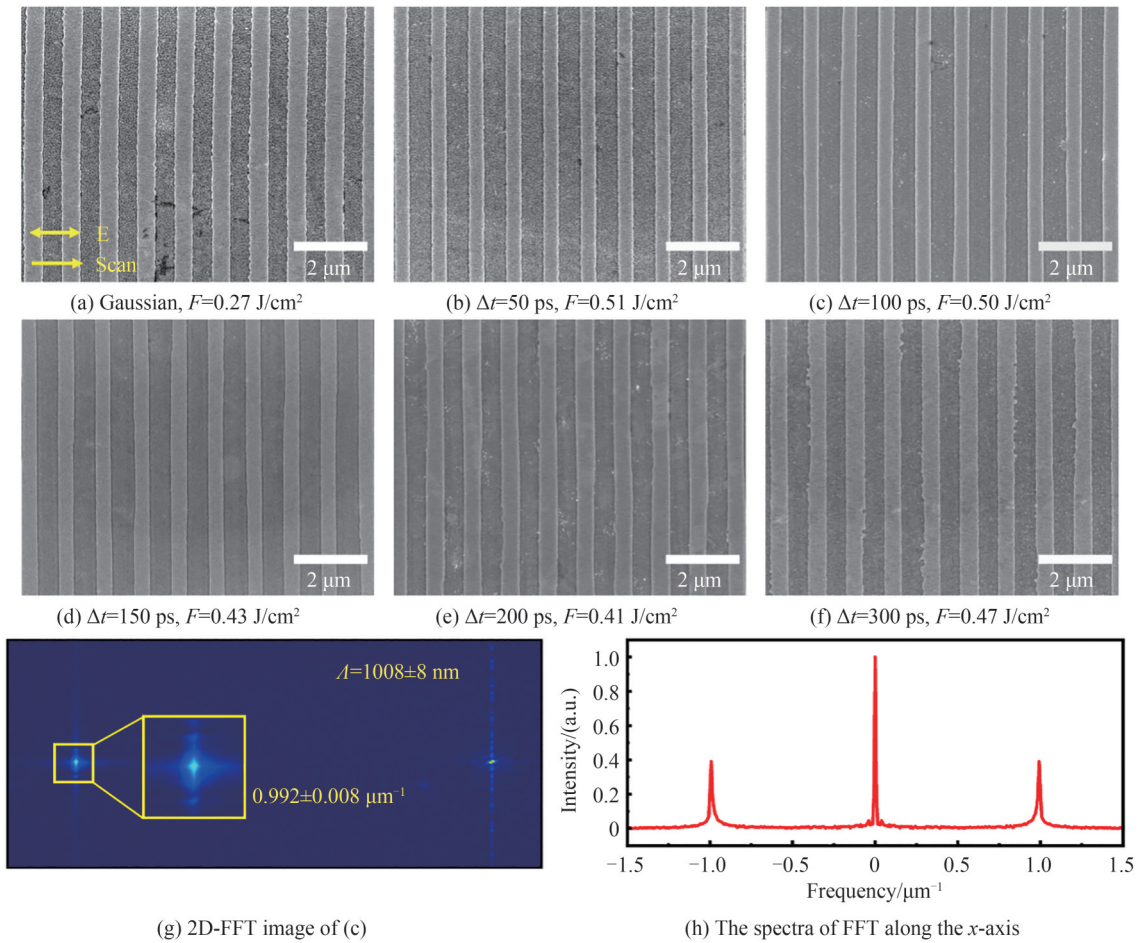
(a) Gaussian, F=0.27 J/cm²   (b) Δt=50 ps, F=0.51 J/cm²   (c) Δt=100 ps, F=0.50 J/cm²

(d) Δt=150 ps, F=0.43 J/cm²   (e) Δt=200 ps, F=0.41 J/cm²   (f) Δt=300 ps, F=0.47 J/cm²

Λ=1008±8 nm

0.992±0.008 μm⁻¹

(g) 2D-FFT image of (c)   (h) The spectra of FFT along the x-axis

图 5 飞秒激光脉冲串诱导均匀 NSRs 的扫描电镜照片,扫描速度为 6 mm/s
Fig.5 SEM images of regular NSRs induced by femtosecond laser pulse train with scanning velocity of 6 mm/s
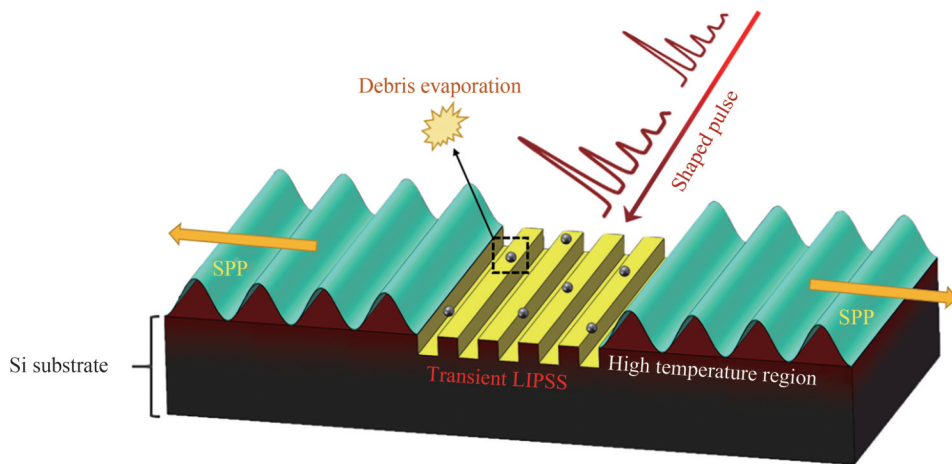

图 6 飞秒激光脉冲串诱导规则 NSRs 原理
Fig.6 Schematic diagram of femtosecond laser pulse train induced regular NSRs

激光脉冲串加工的亚波长条纹均匀排列,条纹规则性高。

　　图 7 为不同子脉冲间隔的飞秒激光脉冲串在硅上诱导不同形貌的 NSRs 的能流密度窗口。子脉冲间隔为 100 ps 的飞秒激光脉冲串诱导规则 NSRs 的能流密度窗口为 0.08 J/cm²(0.43~0.51 J/cm²),是高斯激光脉冲最大能流密度窗口的 4 倍。这意味着在实际的激光加工中,飞秒激光脉冲串诱导规则 NSRs 对激光条件要求低,稳定性更好。
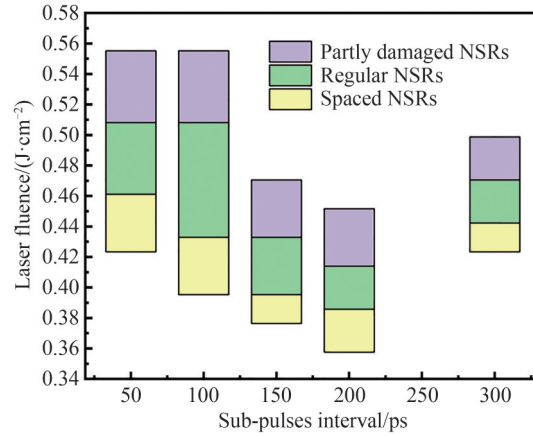
图7 飞秒激光脉冲串在硅上诱导不同形貌NSRs的能流密度窗口,扫描速度为6 mm/s

Fig.7 Laser fluence window of NSRs induced by femtosecond laser pulse train on silicon with scanning velocity of 6 mm/s

2.3 NSRs深度

NSRs深度是影响表面结构色、衍射效率、偏振特性[39, 40]的重要因素。图8(a)、(b)为图5中高斯激光脉冲和子脉冲间隔100 ps脉冲串诱导出的NSRs的共聚焦光学显微镜照片,两组照片采用同一种色阶标尺。首先取出条纹上下边界端点的最小值,图8(c)中用蓝色虚线标注水平位置,其余端点与该位置的数值偏差计为条纹深度的起伏。高斯激光脉冲诱导出的NSRs深度为(22±3.2) nm,起伏为14.4%。子脉冲间隔100 ps整形脉冲诱导出的NSRs深度为(45.7±2.7) nm,起伏仅5.9%。利用整形脉冲串加工得到的条纹深度约为原始高斯激光脉冲的2倍,同时深度起伏也大大减小,条纹更加均匀。

图9显示了子脉冲间隔100 ps飞秒激光脉冲串诱导出的NSRs深度与能流密度变化关系。当激光能流

(a) Confocal microscope image of NSRs induced by Gaussian laser pulse
F=0.27 J/cm², v=6 mm/s

(b) Confocal microscope image of NSRs induced by shaped pulse of 100 ps
F=0.51 J/cm², v=6 mm/s

(c) 2D plots of the cross-sections along the yellow arrows in (a)

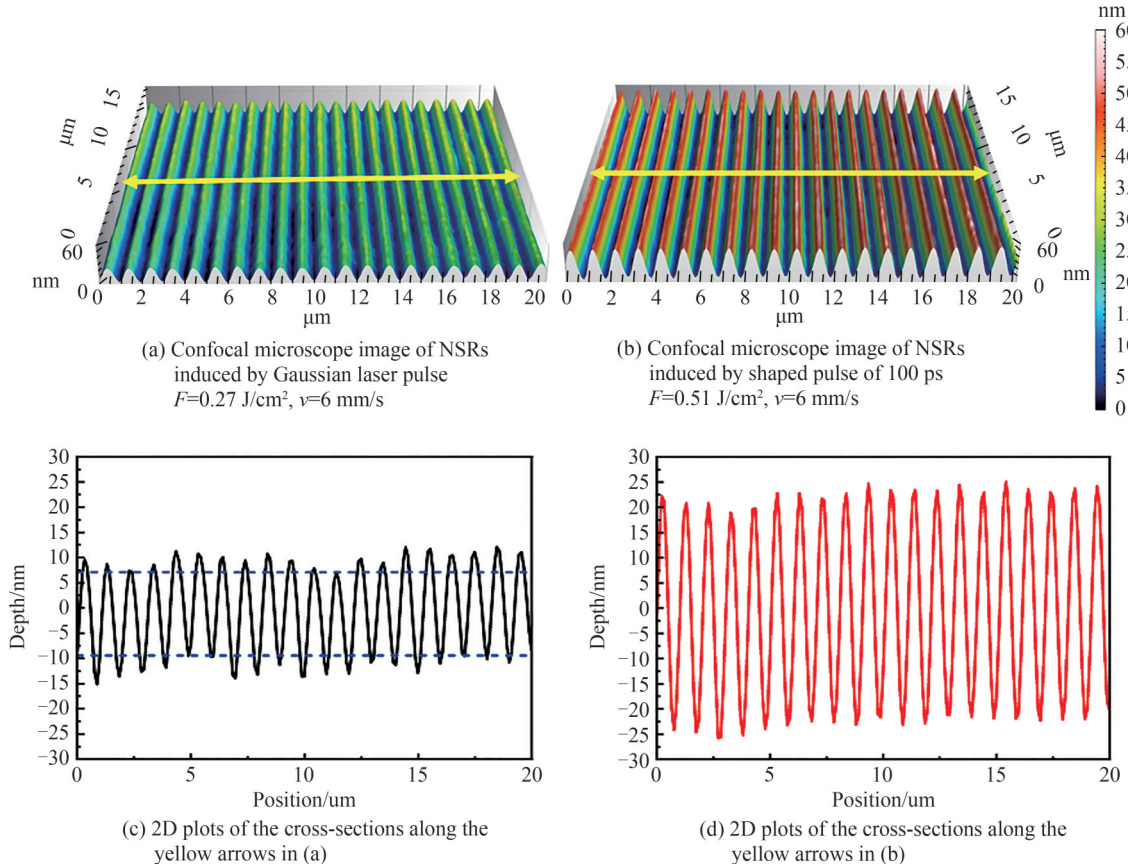(d) 2D plots of the cross-sections along the yellow arrows in (b)

图8 高斯激光脉冲和子脉冲间隔100 ps飞秒激光脉冲串诱导出的NSRs的深度对比

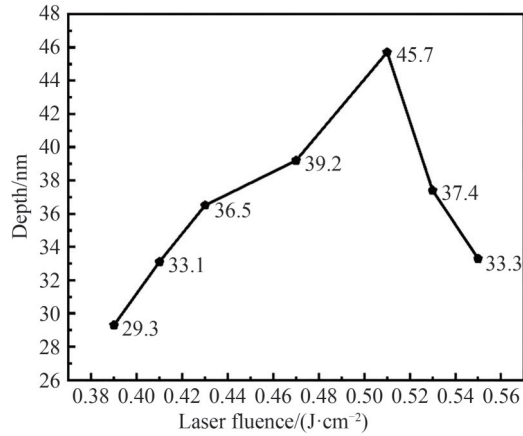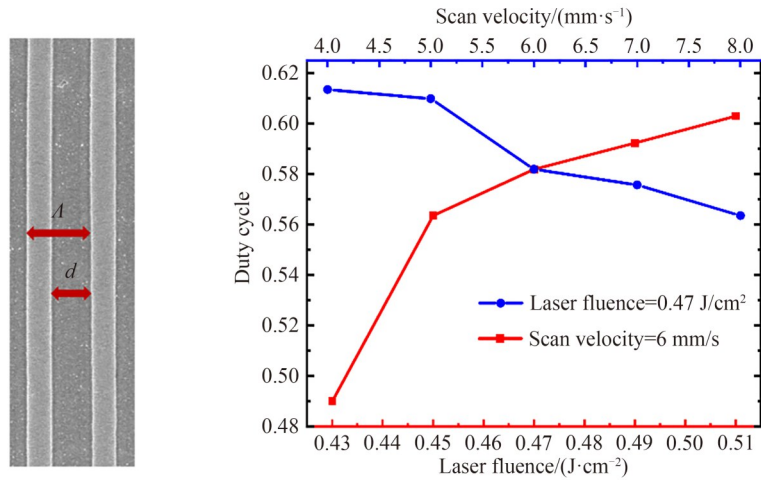Fig.8 Depth comparison of NSRs induced by Gaussian laser pulse and femtosecond laser pulse train of 100 ps

图 9　子脉冲间隔 100 ps 飞秒激光脉冲串诱导出的 NSRs 深度与能流密度变化关系
Fig.9　The relationship between laser fluence and depth of NSRs induced by femtosecond laser pulse train of 100 ps

密度较小时,由于材料表面的能量沉积不足,导致条纹浅,并且均匀性差;随着激光能流密度的增大,在诱导规则亚波长周期条纹的能流密度窗口区,更多的能量沉积使得条纹深度逐渐增加,由 0.43 J/cm² 下的 36.5 nm 增加至 0.51 J/cm² 下的 45.7 nm。当激光能流密度增大到一定数值,由于剩余热效应较大,相邻条纹之间碎屑沉积增多,部分条纹甚至被淹没,深度减小,且深度起伏增大。

2.4　NSRs 占空比

如图 10(a)所示,占空比定义为 NSRs 的底部槽宽度 d 与周期 Λ 之比。图 10(b)显示了不同参数下子脉冲间隔 100 ps 飞秒激光脉冲串诱导出的 NSRs 占空比的变化情况。蓝色实线为激光能流密度为 0.47 J/cm² 时占空比随扫描速度的变化关系,随着扫描速度的增加,材料表面单位面积的脉冲累积数逐渐减少,材料的烧蚀去除相应减少,占空比减小。红色实线为激光扫描速度为 6 mm/s 的条件下占空比随激光能流密度的变化关系,激光能流密度由 0.43 J/cm² 增加到 0.51 J/cm²,较多的能量沉积使得材料的烧蚀去除增加,占空比由 0.49 增加到 0.60。

(a) The definition of duty cycle　　　(b) The duty cycle of NSRs at different parameters

图 10　子脉冲间隔 100 ps 飞秒激光脉冲串诱导出的 NSRs 的占空比分析
Fig.10　Duty cycle analysis of NSRs induced by femtosecond laser pulse train of 100 ps

2.5　NSRs 取向性

结构取向角差异(Divergence of Structure Orientation Angle, DSOA)是指待测结构其角度分布最大值一半处的半宽值 $\delta\theta$。利用 ImageJ 插件 OrientationJ 分别对图 5 中高斯激光脉冲和飞秒激光脉冲串诱导得到的 NSRs 分别进行取向角测量,分析 NSRs 结构局部取向优劣。如图 11(a)所示,高斯激光脉冲诱导得到的 NSRs 的 DSOA 值为 7.9°,而子脉冲间隔 100 ps 整形脉冲诱导得到的 NSRs 的 DSOA 值仅为 2.8°,条纹的一

(a) Distribution of orientation of NSRs in Fig.5 (a, c)
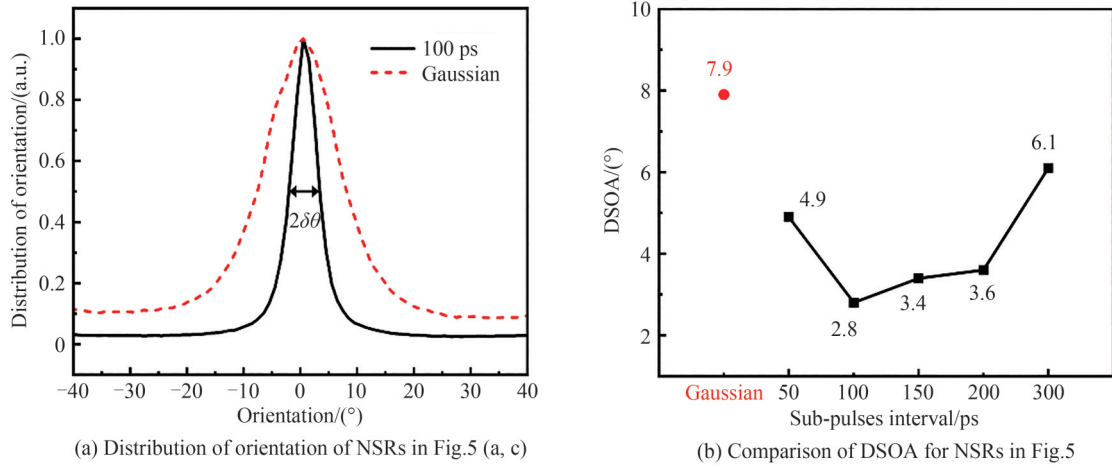
(b) Comparison of DSOA for NSRs in Fig.5

图 11 高斯激光脉冲和飞秒激光脉冲串诱导规则 NSRs 的取向角分析

Fig. 11 DSOA analysis of regular NSRs induced by Gaussian laser pulse and femtosecond laser pulse train

致性明显提升。飞秒激光脉冲串诱导的 NSRs 的 DSOA 值汇总于图 11(b)中,子脉冲间隔 100 ps 整形脉冲为最优整形脉冲。子脉冲间隔 50 ps 整形脉冲诱导得到的 NSRs 的 DSOA 值略大于子脉冲间隔 100 ps 整形脉冲所对应的 DSOA 值,当子脉冲间隔大于 100 ps 时,整形脉冲诱导得到的规则 NSRs 的 DSOA 值逐渐增加,在实验范围内,所有整形脉冲诱导得到的 NSRs 平直度和规则性均优于高斯激光诱导得到的 NSRs。

2.6 NSRs边缘粗糙度

边缘粗糙度(Line Edge Roughness, LER)常用于表征光刻图形边缘的粗糙程度[33],也是飞秒激光诱导规则 NSRs 的重要评价指标之一。利用 Matlab 对图 5 中高斯激光脉冲和飞秒激光脉冲串诱导得到的 NSRs 进行边缘提取,如图 12(a)所示,提取出条纹边缘。通过最小二乘法拟合得到样本平均边缘的一维直线,平均位置计为 $\bar{x}$,读取样本点到拟合边缘的距离 x_i,$x_i - \bar{x}$ 为样本点到拟合边缘的偏差,条纹边缘的标准误差为

$$\sigma_{LER} = \sqrt{\frac{1}{N}\sum_{i=1}^{N}(x_i - \bar{x})^2} \tag{1}$$

式中,σ_{LER} 为边缘粗糙度,N 为样本点个数。分别对单根条纹进行粗糙度分析,得出平均值。图 12(b)为图 5 中不同激光条件下诱导的最规则的 NSRs 的边缘粗糙度,高斯飞秒激光诱导的 NSRs 的边缘粗糙度为

(a) Edge detection

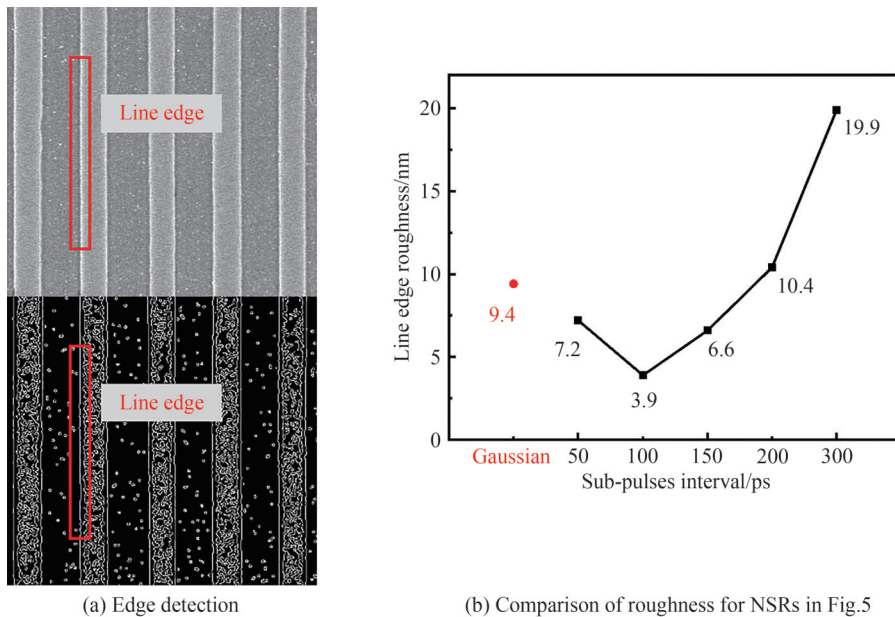(b) Comparison of roughness for NSRs in Fig.5

图 12 高斯激光脉冲和飞秒激光脉冲串诱导规则 NSRs 的边缘粗糙度分析

Fig.12 Edge roughness analysis of regular NSRs induced by Gaussian laser pulse and femtosecond laser pulse train

9.4 nm。在飞秒激光脉冲串诱导下,子脉冲间隔为100 ps的脉冲串诱导得到的NSRs边缘粗糙度最小,为3.9 nm,达到光刻工艺标准。子脉冲间隔50 ps、100 ps和150 ps整形脉冲诱导得到的NSRs边缘粗糙度均小于高斯激光脉冲对应的边缘粗糙度。子脉冲间隔为300 ps的脉冲串诱导时,条纹边沿粗糙度差异较大,出现单边质量较好或者极差的情况,粗糙度平均值较高。

3 结论

本文提出一种高效输出飞秒激光脉冲串的装置——基于F-P腔的脉冲串产生系统,利用子脉冲强度递减的飞秒激光脉冲串在硅表面诱导NSRs。实验结果表明,子脉冲间隔为100 ps的脉冲串能够诱导出周期为1 008 nm,结构取向角为2.8°,边缘粗糙度为3.9 nm的高质量亚波长周期条纹,相较高斯飞秒激光加工,条纹平直度好、深度大、边缘粗糙度小。更多的激光能量周期性沉积和更小的热效应,以及更少的表面沉积颗粒,是飞秒激光脉冲串诱导高质量亚波长条纹的原因。利用F-P腔产生的飞秒激光脉冲串能够显著提升NSRs的加工质量,达到光刻工艺的水平,有望提高传统飞秒激光加工的精度。

参考文献

[1] LIN Z, HONG M. Femtosecond laser precision engineering: from micron, submicron, to nanoscale [J]. Ultrafast Science, 2021, 2021:9783514.

[2] ZHANG Y C, JIANG Q L, CAO K Q, et al. Extremely regular periodic surface structures in a large area efficiently induced on silicon by temporally shaped femtosecond laser [J]. Photonics Research, 2021, 9(5): 839-847.

[3] YANG Q X, LIU H L, HE S, et al. Circular cladding waveguides in Pr:YAG fabricated by femtosecond laser inscription: Raman, luminescence properties and guiding performance [J]. Opto-Electronic Advances, 2021, 4(2): 200005.

[4] JIA T Q, CHEN H X, HUANG M, et al. Formation of nanogratings on the surface of a ZnSe crystal irradiated by femtosecond laser pulses [J]. Physical Review B, 2005, 72(12): 125429.

[5] SHIMOTSUMA Y, KAZANSKY P G, QIU J, et al. Self-organized nanogratings in glass irradiated by ultrashort light pulses [J]. Physical Review Letters, 2003, 91(24): 247405.

[6] BHARDWAJ V R, SIMOVA E, RAJEEV P P, et al. Optically produced arrays of planar nanostructures inside fused silica [J]. Physical Review Letters, 2006, 96(5): 057404.

[7] HOHM S, ROSENFELD A, KRUGER J, et al. Femtosecond laser-induced periodic surface structures on silica [J]. Journal of Applied Physics, 2012, 112(1): 014901.

[8] WANG H T, HAO C L, LIN H, et al. Generation of super-resolved optical needle and multifocal array using graphene oxide metalenses [J]. Opto-Electronic Advances, 2021, 4(2): 200031.

[9] WANG J C, GUO C L. Ultrafast dynamics of femtosecond laser-induced periodic surface pattern formation on metals [J]. Applied Physics Letters, 2005, 87(25): 251914.

[10] CHENG K, LIU J K, CAO K Q, et al. Ultrafast dynamics of single-pulse femtosecond laser-induced periodic ripples on the surface of a gold film [J]. Physical Review B, 2018, 98(18): 184106.

[11] TSUTSUMI N, FUJIHARA A. Pulsed laser induced spontaneous gratings on a surface of azobenzene polymer [J]. Applied Physics Letters, 2004, 85(20): 4582-4584.

[12] REBOLLAR E, DE ALDANA J R V, PEREZ-HERNANDEZ J A, et al. Ultraviolet and infrared femtosecond laser induced periodic surface structures on thin polymer films [J]. Applied Physics Letters, 2012, 100(4): 041106.

[13] DUSSER B, SAGAN Z, SODER H, et al. Controlled nanostructrures formation by ultra fast laser pulses for color marking [J]. Optics Express, 2010, 18(3): 2913-2924.

[14] MARTINEZ-CALDERON M, RODRIGUEZ A, DIAS-PONTE A, et al. Femtosecond laser fabrication of highly hydrophobic stainless steel surface with hierarchical structures fabricated by combining ordered microstructures and LIPSS [J]. Applied Surface Science, 2016, 374: 81-89.

[15] LI Yanli, JIA Xin, CAO Kaiqiang, et al. Highly efficient fabrication of superhydrophilic structures on silicon surface by the interference of two femtosecond laser beams [J]. Acta Photonica Sinica, 2021, 50(6): 0650111.
      李艳丽,贾鑫,曹凯强,等. 飞秒激光双光束干涉高效率地制备硅表面超亲水结构 [J]. 光子学报,2021,50(6): 0650111.

[16] BAI S, SERIEN D, MA Y, et al. Attomolar sensing based on liquid interface-assisted surface-enhanced Raman scattering in microfluidic chip by femtosecond laser processing [J]. Acs Applied Materials & Interfaces, 2020, 12(37): 42328-42338.

[17] ERKIZAN S N, IDIKUT F, DEMIRTAS O, et al. LIPSS for SERS: metal coated direct laser written periodic nanostructures for surface enhanced raman spectroscopy [J]. Advanced Optical Materials, 2022, 10(22): 2200233.

[18] HUANG J, JIANG L, LI X W, et al. Fabrication of highly homogeneous and controllable nanogratings on silicon via chemical etching-assisted femtosecond laser modification [J]. Nanophotonics, 2019, 8(5): 869-878.

［19］ BRICCHI E, KAZANSKY P G. Extraordinary stability of anisotropic femtosecond direct-written structures embedded in silica glass ［J］. Applied Physics Letters, 2006, 88(11): 111119.

［20］ DREVINSKAS R, GECEVICIUS M, BERESNA M, et al. Tailored surface birefringence by femtosecond laser assisted wet etching ［J］. Optics Express, 2015, 23(2): 1428-1437.

［21］ CERKAUSKAITE A, DREVINSKAS R, SOLODAR A, et al. Form-birefringence in ITO thin films engineered by ultrafast laser nanostructuring ［J］. Acs Photonics, 2017, 4(11): 2944-2951.

［22］ HUANG M, ZHAO F L, CHENG Y, et al. Origin of laser-induced near-subwavelength ripples: interference between surface plasmons and incident laser ［J］. Acs Nano, 2009, 3(12): 4062-4070.

［23］ BONSE J, ROSENFELD A, KRUGER J. On the role of surface plasmon polaritons in the formation of laser-induced periodic surface structures upon irradiation of silicon by femtosecond-laser pulses ［J］. Journal of Applied Physics, 2009, 106(10): 104910.

［24］ DERRIEN T J Y, ITINA T E, TORRES R, et al. Possible surface plasmon polariton excitation under femtosecond laser irradiation of silicon ［J］. Journal of Applied Physics, 2013, 114(8): 083104.

［25］ CAO K Q, CHEN L, WU H C, et al. Large-area commercial-grating-quality subwavelength periodic ripples on silicon efficiently fabricated by gentle ablation with femtosecond laser interference via two cylindrical lenses ［J］. Optics and Laser Technology, 2020, 131: 106441.

［26］ JALIL S A, YANG J J, ELKABBASH M, et al. Maskless formation of uniform subwavelength periodic surface structures by double temporally-delayed femtosecond laser beams ［J］. Applied Surface Science, 2019, 471: 516-520.

［27］ WEINER A M, HERITAGE J P, KIRSCHNER E M. High-resolution femtosecond pulse shaping ［J］. Journal of the Optical Society of America B (Optical Physics), 1988, 5(8): 1563-1572.

［28］ JIANG L, WANG A D, LI B, et al. Electrons dynamics control by shaping femtosecond laser pulses in micro/nanofabrication: modeling, method, measurement and application ［J］. Light-Science & Applications, 2018, 7: 17134.

［29］ GIANNUZZI G, GAUDIUSO C, DI FRANCO C, et al. Large area laser-induced periodic surface structures on steel by bursts of femtosecond pulses with picosecond delays ［J］. Optics and Lasers in Engineering, 2019, 114: 15-21.

［30］ DROMEY B, ZEPF M, LANDREMAN M, et al. Generation of a train of ultrashort pulses from a compact birefringent crystal array ［J］. Applied Optics, 2007, 46(22): 5142-5146.

［31］ ZHANG J, WANG S M, JIANG L, et al. Morphology control of nanostructure using microsphere-assisted femtosecond laser double-pulse ablation and chemical etching ［J］. Applied Surface Science, 2020, 502: 144272.

［32］ WANG Z, JIANG L, LI X W, et al. High-throughput microchannel fabrication in fused silica by temporally shaped femtosecond laser Bessel-beam-assisted chemical etching ［J］. Optics Letters, 2018, 43(1): 98-101.

［33］ 韦亚一. 超大规模集成电路先进光刻理论与应用 ［M］. 北京: 科学出版社, 2016.

［34］ CHEN Tianqi, YANG Jian, JIA Tianqing. A study on ablation quality of silicon by femtosecond laser pulse trains ［J］. Acta Photonica Sinica, 2021, 50(6): 0650112.
　　　 陈天琦, 杨坚, 贾天卿. 飞秒激光脉冲序列烧蚀硅的孔型质量研究 ［J］. 光子学报, 2021, 50(6): 0650112.

［35］ DONG Y Y, MOLIAN P. Coulomb explosion-induced formation of highly oriented nanoparticles on thin films of 3C-SiC by the femtosecond pulsed laser ［J］. Applied Physics Letters, 2004, 84(1): 10-12.

［36］ RUDENKO A, MAUCLAIR C, GARRELIE F, et al. Amplification and regulation of periodic nanostructures in multipulse ultrashort laser-induced surface evolution by electromagnetic-hydrodynamic simulations ［J］. Physical Review B, 2019, 99(23): 235412.

［37］ LIU J K, JIA X, WU W S, et al. Ultrafast imaging on the formation of periodic ripples on a Si surface with a prefabricated nanogroove induced by a single femtosecond laser pulse ［J］. Optics Express, 2018, 26(5): 6302-6315.

［38］ HASHIDA M, SEMEROK A F, GOBERT O, et al. Ablation threshold dependence on pulse duration for copper ［J］. Applied Surface Science, 2002, 197: 862-867.

［39］ HUANG J, JIANG L, LI X W, et al. Cylindrically focused nonablative femtosecond laser processing of long-range uniform periodic surface structures with tunable diffraction efficiency ［J］. Advanced Optical Materials, 2019, 7(20): 1900706.

［40］ WU H, JIAO Y L, ZHANG C C, et al. Large area metal micro-/nano-groove arrays with both structural color and anisotropic wetting fabricated by one-step focused laser interference lithography ［J］. Nanoscale, 2019, 11(11): 4803-4810.

High Quality Near-subwavelength Ripples on Si Induced by Femtosecond Pulse Train Output from Fabry-Perot Cavity(Invited)

XU Yufeng, ZHANG Yuchan, JIANG Qilin, SHEN Huihui, JIA Tianqing

(*State Key Laboratory of Precision Spectral Science and Technology, East China Normal University, Shanghai* 200241, *China*)

Abstract:Laser-Induced Periodic Surface Structures(LIPSS) can be widely used in different processing fields, involving various materials such as semiconductors, dielectrics, metals, polymers. They have great potential in micro-nano processing. LIPSS are divided into two categories:Near-Subwavelength Ripples (NSRs) with period Λ larger than $\lambda/2$ and Deep-Subwavelength Ripples(DSRs) with period Λ smaller than $\lambda/2$, where λ is the incident laser wavelength. LIPSS can improve the surface properties of materials and can be used for modulation of the surface wettability of materials; enhanced surface Raman scattering; surface coloring; birefringence and optical storage, etc. They can be widely applied in many fields such as data storage, industrial manufacturing, and biomedicine.

The formation of LIPSS is a complex process. Within a few nanoseconds after the femtosecond laser irradiation on the material surface, a series of ultrafast processes such as carrier excitation, carrier heating, lattice heating, plasma ejection, and nanoparticle ejection occur, which greatly increases the difficulty of processing regular NSRs. Therefore, how to improve the quality of NSRs has been an important research direction for femtosecond laser processing.

Pulse shaping can regulate the distribution of laser energy in the time domain, which can then regulate the ultrafast process of laser-matter interaction. In order to fabricate high-quality LIPSS, we built a Fabry-Perot(F-P) cavity femtosecond laser pulse train processing system to conduct femtosecond laser time-domain shaping. The central wavelength of the laser is 1 030 nm, and we output femtosecond laser pulse train with flexible sub-pulse intervals in the range of 1~300 ps to fabricate NSRs on the silicon surface. The laser scanning velocity is altered by moving the sample through a 3D electronically controlled translation stage. By adjusting the distance between beam splitter and zero-degree mirror, we changed the sub-pulse interval and investigated NSRs induced by pulse trains with different sub-pulse intervals.

After the samples were processed, we tested the surface morphology of the samples using a Scanning Electron Microscope(SEM). The NSRs induced by a Gaussian laser were slightly curved and had rough edges. However, the NSRs induced by the shaped pulse with a sub-pulse interval of 100 ps were uniformly oriented with smooth and straight edges. The peak of the spectrum obtained by its Fourier transform was (0.992 ± 0.008) μm^{-1}, corresponding to the period $\Lambda=(1\ 008\pm8)$ nm. The laser fluence window of the NSRs induced by the shaped pulse with a sub-pulse interval of 100 ps was 0.08 J/cm^2, which was four times as large as the NSRs induced by the Gaussian laser pulse. As the sub-pulse interval increased, regular NSRs could also be induced, but the width of single ripples was not uniform and the ripples started to become curved with inconsistent orientation. The surface morphology and depth of the sample were measured using a white light interference confocal microscope. The depth of regular NSRs induced by Gaussian laser pulse was (22 ± 3.2) nm, and the depth fluctuation reached 14.4%. In contrast, the depth of regular NSRs induced by the pulse train of 100 ps was (45.7 ± 2.7) nm, and the depth fluctuation was only 5.9%. The depth of NSRs induced by shaping pulse train was about twice that of the original Gaussian laser pulse. Meanwhile, the depth fluctuation was greatly reduced and the ripples were more regular. We used the ImageJ plug-in OrientationJ to measure the Divergence of Structure Orientation Angle(DSOA) of NSRs induced by Gaussian laser pulse and F-P cavity shaping pulses, and then analyzed the local orientation. The DSOA of the NSRs induced by Gaussian laser pulse was 7.9°, while the DSOA of the NSRs induced by pulse train of 100 ps was only 2.8°. The straightness and regularity of NSRs induced by all pulse trains were better than those induced by Gaussian laser pulse in the experimental range, which indicated that the NSRs induced by pulse trains were straight and regular. To quantitatively calculate the line edge roughness of the NSRs, we performed edge detection on the NSRs induced by different conditions. We obtained the one-dimensional straight line of the sample-averaged boundary by least-squares fitting and calculated the standard error of the line edge. The best NSRs induced by pulse train of 100 ps had an edge roughness of 3.9 nm, which could meet the standard of lithography process.

In summary，NSRs induced by the femtosecond laser pulse train is superior to the NSRs induced by Gaussian laser pulse. The flatness，depth，and edge roughness of NSRs are significantly improved. Femtosecond laser pulse train can improve the quality of NSRs. Laser pulse shaping is expected to overcome the thermal effects，ejected particles and insufficient energy deposition during femtosecond laser processing and improve the processing accuracy.